Defense Technical Information Center Compilation Part Notice

ADP012258

TITLE: The Coercivity - Remanence Tradeoff in Nanocrystalline Permanent Magnets

DISTRIBUTION: Approved for public release, distribution unlimited

This paper is part of the following report:

TITLE: Nanophase and Nanocomposite Materials IV held in Boston, Massachusetts on November 26-29, 2001

To order the complete compilation report, use: ADA401575

The following component part numbers comprise the compilation report:
ADP012174 thru ADP012259

Mat. Res. Soc. Symp. Proc. Vol. 703 © 2002 Materials Research Society U2.8

The Coercivity – Remanence Tradeoff in Nanocrystalline Permanent Magnets

Laura H. Lewis and David C. Crew
Materials and Chemical Sciences Division, Energy Sciences and Technology Dept.,
Brookhaven National Laboratory, Upton, New York 11973-5000 USA

ABSTRACT

The energy product $(BH)_{max}$ is a figure of merit quantifying the maximum amount of useful work that can be performed by the magnet. The energy product is determined by the magnetic remanence and the coercivity which, as extrinsic properties, are determined by the magnets' microstructure. Thus, in principle, magnetic material microstructures may be tailored to obtain defined parameters to produce optimal permanent magnets. However, as asserted by the eponymous Murphy, "Nature favors the hidden flaw". While there is still much undeveloped potential in nanomagnetic materials, with relevant length scales on the order of 100 Å, accumulating evidence strongly suggests that maximum remanence and maximum coercivity are mutually exclusive in nanocrystalline magnetic materials. Diverse experimental and computational results obtained from nanocrystalline $Nd_2Fe_{14}B$-based magnets produced by melt-spinning techniques and subjected to various degrees of thermomechanical deformation confirm this conclusion. Recent results obtained from temperature-dependent magnetic measurement, magnetic force microscopy and simple micromagnetic modeling will be reviewed and summarized. The results, while somewhat discouraging, do hint at possible materials design routes to sidestep the inherent performance limitations of the magnetic nanostructures.

INTRODUCTION

The permanent magnet material $Nd_2Fe_{14}B$ in its nanocrystalline form exhibits very favorable properties conferred by the rapid solidification process: simplified processing, good corrosion resistance and high magnetic hardness provided by a nanoscale grain size on the order of 200 nm. The metallurgical properties of the $Nd_2Fe_{14}B$ compound allow it to be thermomechanically deformed, or "die-upset", a process that significantly improves the remanence B_r of the magnet [1]. This increase in remanence results stems from two effects: (a) the exchange enhancement of the magnetization in the intergranular regions [2] and (b) an increased degree of crystallographic texture of the magnet. Both effects enhance the energy product $(BH)_{max}$, which is a figure of merit that quantifies the maximum amount of useful work that may be performed by the magnet. The energy product is determined by the magnetic remanence and the coercivity which, as extrinsic properties, are largely determined by the magnets' microstructure. Thus, in principle, it should be possible to tailor magnetic material microstructures to obtain target properties that yield optimal permanent magnets.

Unfortunately, the increase in the remanence upon die-upsetting is always accompanied by a decrease in the coercivity H_{ci} of the magnet. The reasons underlying this phenomenon are unclear. This coercivity decrease dilutes the gains in the energy product produced by the increased remanence and, in some cases, limits the range of applications of the magnet. This decrease in coercivity with increasing level of deformation is in contrast to that expected from an archetypal assemblage of Stoner-Wohlfarth particles that reverse by ideal coherent rotation. The

Stoner-Wohlfarth model, applicable only to homogenous systems of magnetically-isolated uniaxial single-domain particles, yields a coercivity $H_C(\theta)$ as a function of angle θ between the magnetic easy axis and the applied field that increases with decreasing θ according to the Eq. [3]

$$H_c(\theta)/H_c(\theta=0) \approx \left(\cos^{2/3}\theta + \sin^{2/3}\theta\right)^{-1/2} \qquad (1)$$

Results of the Stoner-Wohlfarth model imply that nanocrystalline assemblages with $\theta < 45°$ will exhibit increasing coercivity with decreasing angle θ. The model complementary to the Stoner-Wohlfarth model is the Kondorsky pinning model [4] which predicts coercivity to vary with θ as $1/\cos\theta$, where θ again is the angle of the easy axis of the grain with respect to the applied field direction. The physical origins of the Kondorsky model lie in the fact that when the coercivity is low relative to the anisotropy field, as in most advanced permanent magnets, field-induced rotation of the moments out of the easy axis may be neglected. In this situation, magnetic reversal is accomplished by the component of applied field acting along the easy axis of a given grain. Crystallographic grain alignment allows the easy axes of an ensemble of magnetic particles to be rotated by a smaller angle θ with respect to the field. This action results in an increased component of the field acting upon the grain that produces an overall coercivity decrease because the mean coercivity of the grains decreases.

Results computed with the Stoner-Wohlfarth model or the Kondorsky pinning model are in contradiction to behavior observed in die-upset nanocrystalline magnets (Fig. 1), although Givord [5] reports on the existence of similar work by Viadieu that does appear to conform to a $1/\cos\theta$ trend. Fig. 1 shows the correlated, but non-monotonic, relationship between the coercivity and the degree of crystallographic alignment, as quantified by the half-width at half-maximum (HWHM) value of a x-ray diffraction rocking curve for a series of $Nd_2Fe_{14}B$-based die-upset samples with nominal composition $Nd_{13.9}(Fe_{0.92}Co_{0.08})_{80.3}B_{5.3}Ga_{0.5}$ that were deformed to varying degrees [6]. The level of deformation (%) as given in Fig. 1 is the percent change in original height upon deformation.

It is generally accepted that the presence of significant intergranular interactions annul application of the Stoner-Wohlfarth model in nanocrystalline magnets. As summarized by Givord [4], computational models indicate that the field at which magnetic reversal occurs decreases with increasing intergranular exchange. However, the effect of relative crystallographic alignment between constituent nanograins on the magnetic reversal in such materials is less clear. The modeled behavior of two exchange-coupled grains with one grain misaligned by 65° with respect to the applied field [7] indicate that the coercive field of grains coupled by both dipolar and exchange interactions decreases for large granular misalignment, inconsistent with

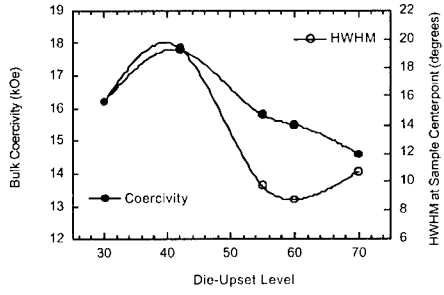

Figure 1. Bulk coercivity and (006) $Nd_2Fe_{14}B$ Bragg reflection rocking curve HWHM data as a function of magnet die-upset level.

experimental observations (Fig. 1). Clarification of the tradeoff in magnetic property optimization with crystallographic alignment of constituent nanograins lies in the relationship between the nanocrystalline grain size and the magnetic exchange, as communicated by the magnetic exchange length L_{ex}^{0}:

$$L_{ex}^{0} \approx \sqrt{\frac{A}{K_1}} \tag{2}$$

where A is the exchange stiffness and K_1 is the first-order anisotropy constant [8]. The magnetic exchange length describes the thickness of the magnetization transition existing near an interface, where the magnetization direction can deviate from the defined direction existing in the bulk region of a given grain. In the absence of a perpendicular magnetization component across the interface L_{ex}^{0} may be related to the domain wall width δ_{DW} as [9]:

$$L_{ex}^{0} \approx \frac{\delta_{DW}}{\pi} \tag{3}$$

The room-temperature value of the magnetic exchange length L_{ex}^{0} in $Nd_2Fe_{14}B$ is extremely small, around 21 Å [10]. Further reduction in the magnetic exchange length from its base value is realized from the presence of a perpendicular magnetization component at the interface between nanograins. In this manner a connection between crystallographic alignment and exchange coupling in nanocrystalline magnetic materials is realized.

It is postulated that the magnetic exchange length controls the magnetic behavior in nanocrystalline magnets. When the average grain size of a ferromagnet is much larger than the exchange length, the magnetization deviation at the grain perimeters does not significantly effect the micromagnetics of the system. In such cases the coercivity of the system is largely controlled by lattice imperfections and grain boundary defects, such as a rough grain boundary topography, that furnish regions more susceptible to magnetic reversal relative to the bulk. However, when the grain size descends to the nanoscale the exchange length becomes important; under its influence spins at the peripheries of neighboring nanograins become strongly exchange-coupled. As the relative crystallographic orientation difference between nanograins decreases the intergranular exchange length increases. As the intergranular exchange length increases the local magnetization deviation is likewise reduced, producing a more-uniform micromagnetic state. The exchange-coupling effectively erases the distinction between nanocrystalline grains and decreases the efficacy of the physical grain boundaries to act as barriers to domain wall motion. The peripheral spins on the edges of the nanocrystalline grains constitute a large volume fraction of the total number of spins in the grain; this situation results in magnetic behavior that is very different from that found in the larger-grained counterparts.

Some remarkable phenomena are induced by intergranular exchange coupling in nanocrystalline materials. As the grain size is reduced below the single domain limit intergranular exchange interactions act to bind the magnetic grains into larger units known as "interaction domains", schematically depicted in Fig. 2. These interaction domains, which represent the reversing units of the magnetic structure, can consist of ten to thousands of individual grains. It is important to note that interaction domains may support a domain wall, whereas the individual grains that constitute the interaction domain are typically too small to do so. The scale of the magnetic microstructure, *i.e.*, the size of the interaction domains in nanocrystalline magnets, is

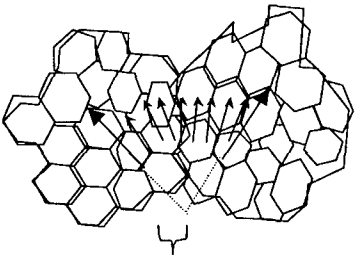

$\Psi < 90°$

Figure 2. Schematic representation of two multi-grain "interaction domains", delineated by the bold outline. The bold arrows indicate the average anisotropy direction of the interaction domains, and the spin rotation angle Ψ is less than 90°.

dependent upon many factors, including the type and magnitude of the magnetocrystalline anisotropy of the compound, the chemical homogeneity and the crystallographic alignment of the constituent grains. Interaction domains are delineated by rotational spin transitions that are distinct from the more-familiar Bloch domain walls found in large-grained materials with magnetization rotations of 180° or 90°. The magnetization transition from one interaction domain to the next subtends an angle Ψ between the collective anisotropy directions of adjacent interaction domains; Ψ is typically less than 90 degrees. It is hypothesized that this divergence in the magnetization is too small to effectively impede domain wall motion.

The above-described factors underlie the structure-sensitive magnetic properties such as coercivity and remanence in nanocrystalline permanent magnet materials and make them unique from their micron-scale counterparts. While there is still much undeveloped potential in nanocrystalline permanent magnet materials, accumulating evidence strongly suggests that the existence of optimal remanence and coercivity are mutually exclusive in nanocrystalline magnetic materials. The microstructural condition found in these materials — that the nanometer grain size is approximately the same size or smaller than the exchange length in $Nd_2Fe_{14}B$ — is hypothesized to underlie this conclusion.

The following sections of this paper present experimental and simple computational results obtained from recent studies of melt-quenched $Nd_2Fe_{14}B$ materials that indicate high remanence and high coercivity seem to be mutually exclusive in nanocrystalline magnets. This conclusion is supported by evidence of increasing magnetic exchange concurrent with increasing grain alignment in nanocrystalline magnets. Investigations of the effect of grain alignment and interaction domain size on coercivity were carried out on a series of $Nd_2Fe_{14}B$-based samples with nominal composition $Nd_{13.9}(Fe_{0.92}Co_{0.08})_{80.3}B_{5.3}Ga_{0.5}$ that were die-upset to varying degrees. The small grain size of these materials guarantees that a significant portion of the constituent atoms reside near grain surfaces and thus these materials represent a good opportunity to examine the effect of intergranular exchange interactions and relative grain alignment upon the magnetic reversal process. A secondary, but still important, microstructural parameter is the change in nanograin shape from quasi-spherical to platelet-type produced by the die-upsetting process. This shape change, while complex and highly nonuniform, nevertheless influences the magnetic coupling and local magnetic reversal mechanism operative in the magnet. In this report the influence of intergrain magnetic exchange coupling on the reversal mechanism and micromagnetic structure in this set of materials is studied with three different techniques: temperature-dependent magnetic measurement [11], magnetic force microscopy [12] and simple micromagnetic modeling [13]. The results, while perhaps discouraging, do hint at possible materials design routes to sidestep the inherent performance limitations of the permanent magnetic nanostructures.

COERCIVITY AND CRYSTALLOGRAPHIC ALIGNMENT RELATIONS

Information concerning the nature and extent of cooperative magnetic reversal in magnets of differing degrees of intergranular alignment may be obtained from measurements of the coercivity as a function of temperature. A number of approaches have been developed in an attempt to quantify the relationship between microstructure and coercivity. The coercivity is phenomenologically described [14,,15 ,16] as a function of the anisotropy field reduced by dipolar interactions within the material:

$$H_c(T) = \alpha(T) \cdot H_a(T) - 4\pi N_{eff} M_S(T) \qquad (4)$$

with the temperature-dependent parameters $H_c(T)$ (coercivity), $H_a(T)$ (anisotropy field) and $M_s(T)$ (saturation magnetization). The parameter $\alpha(T)$ describes the reduction in coercivity due to the existence of a non-ideal microstructure; in a simplistic sense $\alpha(T)$ characterizes the misalignment of the grains. The parameter N_{eff} is an effective demagnetization factor that encompasses both dipolar interactions and the effects of the demagnetization field at grain corners that tend to assist magnetic reversal and reduce the coercivity. Both $\alpha(T)$ and N_{eff} are expected to decrease as the degree of intergranular alignment increases.

Values of $\alpha(T)$ and N_{eff} were determined by measuring a series of hysteresis loops (H_{max}=50 kG) for the die-upset $Nd_2Fe_{14}B$-based samples with increasing temperature from 100 K to room temperature. The samples studied were the previously-mentioned die-upset materials deformed to 0, 30, 42, 55, 60 and 70% reductions in the original sample heights. Using Eq. (4) and plotting H_c/M_s *vs.* H_a/M_s as a function of temperature, the parameters α and N_{eff} were determined by fitting the data to a straight line. The values of H_a used in Eq. (4) were taken from the paper of Grossinger *et al.* [17] and $M_s(T)$ was calculated by extrapolating the high field data. The results for the plots of H_c/M_s *vs.* H_a/M_s for all samples were linear and gave well characterized values of α and N_{eff}, as evidenced by the data for the 0, 30 and 70% deformed samples shown in Fig. 3, with resulting values of α and N_{eff} are shown in Fig. 4. The samples are labeled by the degree of die-upset with the corresponding remanence ratio (M_r/M_s) given in parentheses. The trend of decreasing coercivity with increased crystallographic alignment is indicated on the figure by the arrow. Also shown in Fig. 3 for comparative purposes is data from the work of Hirosawa and Tsubokawa [16] for sintered $Pr_2Fe_{14}B$-based magnets with varying degrees of particle alignment, labeled by the remanence ratio (M_r/M_s).

Fig. 3 shows a distinct linkage between α and N_{eff} as the degree of alignment is varied in both the die-upset samples and the sintered samples. However, the data from the die-upset samples display a trend with coercivity *opposite* to that displayed by the sintered data. The sintered data show the expected Kondorsky-type coercivity behavior, *i.e.* as the degree of alignment is increased the coercivity decreases; additionally α and N_{eff} also decrease in these samples with increasing alignment. While the melt-quenched data also show a decrease in coercivity with increasing alignment, the trend is accompanied by an *increase* in α and N_{eff}, contrary to expectation. An explanation of the observed behavior of α and N_{eff} with increased thermomechanical deformation, and hence increased crystallographic alignment, in nano-crystalline materials is provided based on consideration of the active intergrain exchange interaction. Large-grained materials, such as commercial sintered NdFeB magnets, have small

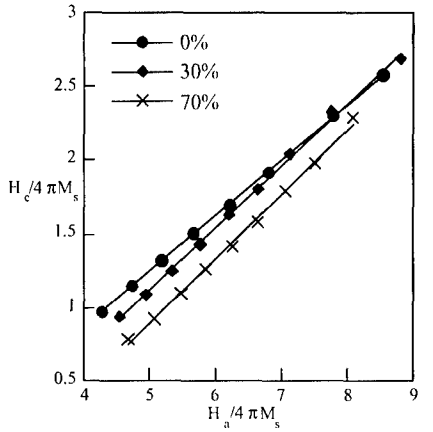

Figure 3. $H_c/4pM_S$ *vs.* $H_a/4pM_S$ for the 0%, 30% and 70% die upset samples. The lines shown are the lines of best fit used to determine α and N_{eff} from Eq. (3).

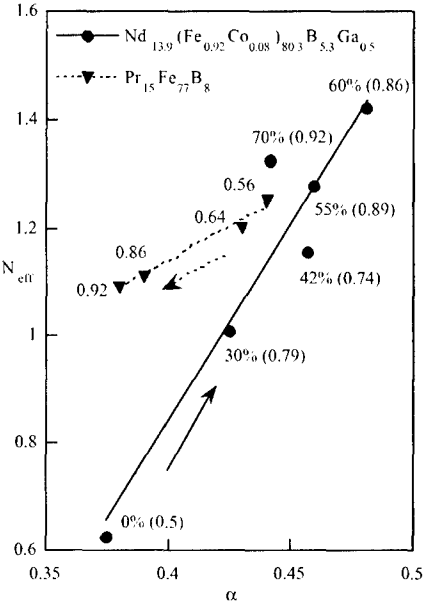

Figure 4. N_{eff} *vs.* α for the melt-quenched NdFeB samples and for a set of sintered PrFeB samples studied by Hirosawa and Tsubokawa [16]. The numerical labels are described in the text. The trend of decreasing coercivity is shown by the arrows

intergrain exchange interactions which favor individual reversal of each grain and provide a coercivity deter mined by the mean coercivity of the individual grains. The coercivity in nanocrystalline materials is determined by a minimum local coercivity which causes reversal of the entire magnet through exchange-coupled avalanche-type magnetization reversal. Thus in these materials the microstructural parameter α is expected to remain relatively unchanged as the degree of crystallographic alignment is increased, because the coercivity is determined by those grains with small orientations to the applied field direction. It is proposed that the coercivity still decreases, despite an approximately constant α in these materials, because nanograin shape changes accompanying the die-upsetting process contribute to increased local stray field configurations that override the expected stray field reduction accompanying grain alignment. The creation of euhedral platelet grains from initially quasi-spherical grains amplifies the stray field gradients at grain corners and triple-point junctions, causing N_{eff} to increase with increasing deformation level. It is hypothesized that only a small population of deformed nanograins is necessary to cause global magnetic reversal because the reversal is rapidly propagated throughout the magnet, underscoring the effect of the intergranular exchange interactions on the coercivity. In summary, remanence increases with deformation, because of greater granular alignment and increased exchange interactions, but these same exchange interactions, combined with other microstructural changes, cause the coercivity to decrease. Thus there is a tradeoff in the two parameters.

COOPERATIVE MAGNETIC BEHAVIOR OBSERVED WITH MAGNETIC FORCE MICROSCOPY

The character and extent of the intergrain magnetic exchange found in nanocrystalline magnets may be inferred from magnetic domain images. Magnetic force microscopy (MFM) was employed to compare the magnetic domain structure in two well-characterized samples of melt-quenched $Nd_2Fe_{14}B$, one sample hot-pressed (isotropic; 0% die upset) and one sample die-upset to a deformation level of 70%. Images of the domain configurations obtained in different magnetic states from these two microstructurally-distinct samples provide information about the effect of intergranular alignment on the magnetic exchange. MFM samples were prepared from 5 mm cubes cut from the center of the samples; one surface of each cube was polished and examined with the surface normal parallel to the press direction. MFM examination of the domain structures of the samples was performed with a Digital Instruments Nanoscope III using standard low coercivity (commercial MESP-LC) tips. The samples were examined in different remanent magnetic states after magnetization to varying levels in a SQUID magnetometer with a 50 kG superconducting magnet.

The nanoscale grain structure of the samples leads to a complex micromagnetic state that has unique MFM contrast. In this work it is deduced that the use of low-coercivity MESP-LC tips to image nanoscale domain structures produces domain contrast rather than the domain wall contrast. This conclusion is discussed in more detail in recent work [12].

MFM images of the hot-pressed material are shown in Figure 5 for three different magnetic states. In the thermally-demagnetized condition (Fig 5a) the image reveals no large-scale structure. A fine-scale contrast is evident with features approximately 150 - 300 nm, which is 2 ~ 3 times the grain size observed by atomic force microscopy. This sample was then saturated in a 50 kG field and imaged in the remanent state (Fig 5b), with remanent magnetic features that are similar in scale to those seen in the thermally-demagnetized condition. A magnetic field of 19.5 kOe was then applied opposite to the remanent magnetization of the sample and then removed, leaving the sample in a DC-demagnetized state (Fig 5c) as confirmed by the near-zero magnetization of the sample measured by SQUID magnetometry. The features observed in the DC-demagnetized state are similar to those seen in the remanent state. MFM images from the

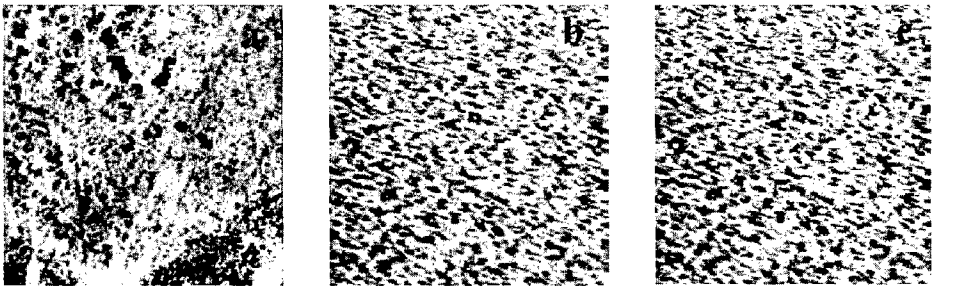

Figure 5: MFM images of hot-pressed $Nd_{13.9}(Fe_{92}Co_8)_{80.3}B_{5.5}Ga_{0.5}$. The image areas are 15 μm by 15 μm. a) Thermally-demagnetized state. b) Remanent state after application of 50 kOe field. c) Coercive state after application and removal of 19.5 kOe reversing field. The press direction is perpendicular to the image plane.

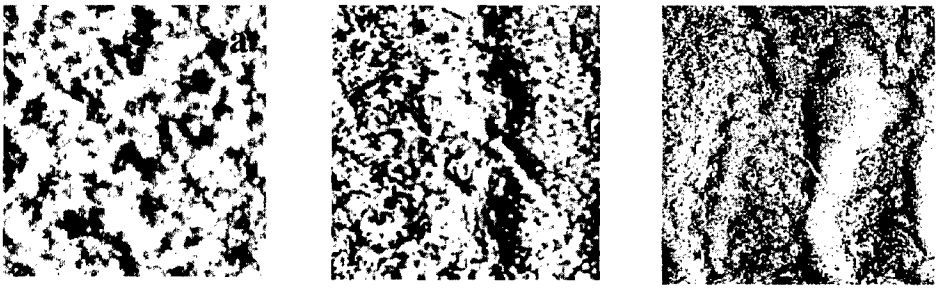

Figure 6: MFM images of thermomechanically-deformed (die-upset) sample $Nd_{13.9}(Fe_{92}Co_8)_{80.3}B_{5.5}Ga_{0.5}$. a) Thermally demagnetized state; image size 15 μm by 15 μm. b) Coercive state after application and removal of a 13.4 kG reversing field; image size 15 μm by 15 μm. c) Same area of the sample as b) except the image size is 50 μm by 50 μm. The press direction is perpendicular to the image plane.

die-upset sample are shown in Fig. 6. The scale of the magnetic structure of the die-upset sample is significantly larger in the thermally-demagnetized condition (Fig 6a)) than in the hot-pressed sample (Fig. 5a)). The magnetic contrast of the die-upset sample is on a scale of 1-2 μm with a finer contrast, on the order of 200 nm, evident within the larger-scale contrast. The fine scale structure is 2-3 times larger than the grain size observed with AFM, but is still 5-10 times smaller than the large scale contrast. It is hypothesized that the observed fine-scale MFM contrast is due to small clusters of exchange-coupled grains within the material, while the larger-scale contrast arises from the coalescence of several magnetic clusters with similar magnetization orientations that create an interaction domain. Application and removal of a reverse field of 13.4 kG to the remanent state drove the sample to a DC-demagnetized state that resulted in a significant change in the domain configuration. The fine-scale magnetic domain structure shown in Fig. 6b) is of a similar scale to the fine-scale structure observed in the thermally-demagnetized condition (*i.e.* approximately 200 nm). However, the image of a larger area, shown in Fig. 6c) and obtained from the same region of the sample as fig. 6b), demonstrates the existence of elongated interaction domains that extend 50 μm or more perpendicular to the magnetization.

In both samples the inherent intergranular exchange interaction is manifest in the finest-scale magnetic contrast, postulated to arise from individual magnetic clusters in the size range 150 - 300 nm that correspond to a volume of approximately 10 exchange-coupled grains. Henceforth the term "cluster" will be used to refer to this fine-scale magnetic contrast, while the term "interaction domain" will be reserved for groups of clusters with similar magnetization orientations existing on length scales of 1 μm to greater than 50 μm. In the hot-pressed material the size of the magnetic cluster domains changes only slightly between thermally-demagnetized, remanent and DC-demagnetized states, indicating that magnetic reversal occurs individually for each cluster. The absence of large multi-cluster interaction domains upon DC-demagnetization in the hot-pressed sample suggest that nucleation of magnetic reversal likely occurs homogeneously throughout the material and the magnetic state of neighboring clusters has only a small effect on cluster reversal. The lack of large interaction domains in the hot-pressed sample is attributed to isotropic crystallographic orientation of the constituent grains. This random crystallographic orientation supplies a perpendicular magnetization component to the cluster interface that reduces the original intergrain magnetic exchange length and ensures small magnetic clusters. In contrast, while the die-upset material exhibits small interaction domains (~ 1-2 μm) in

the thermally-demagnetized condition Figs. 6b) and 6c) indicate the presence of very large interaction domains, extending over 50 μm or more, in the DC-demagnetized condition of this material. It is concluded upon reversal from magnetic saturation the exchange interactions force the reversal of one grain cluster to accelerate the reversal of neighboring clusters. Magnetic reversal in this material thus probably proceeds by a combination of reversal of clusters of grains existing at the peripheries of reversed regions and by an avalanche-type reversal of many clusters simultaneously. Supporting magnetic measurements [18] suggest that magnetic reversal occurs mostly via nucleation of clusters of grains at the peripheries of already-reversed interaction domains, rather than by domain wall unpinning and propagation. The large interaction domains within the die-upset material indicate that the constituent grains with a low coercivity influence the reversal of the entire material to a much greater degree than do similar grains in the hot-pressed material. This effect is, again, attributed to the increased degree and extent of intergranular exchange coupling that accompanies crystallographic alignment in nanocrystalline materials. These measurements show that as alignment proceeds and remanence increases, exchange interactions act to bind grains into larger reversing units. Larger reversing units result in the need for fewer nucleation sites to attain full magnetic reversal and the coercivity decreases as a result.

COERCIVITY AND CRYSTALLOGRAPHIC ALIGNMENT RELATIONS FROM MICROMAGNETIC MODELLING

While previous micromagnetic studies [19, 20] of nanocrystalline magnetic material have largely concentrated on the influence of grain size and phase composition on the bulk magnetic properties, simple computational models may also provide useful information concerning the effect of crystallographic grain alignment on the coercivity of nanocrystalline magnetic materials. In the present work a micromagnetic model has been used to investigate the influence of grain texture upon the scale of the magnetic structure during reversal.

Micromagnetic calculations were performed using a modified version of the 2-dimensional Object Oriented Micromagnetic Framework (OOMMF) software available from NIST [21]. In this model, 3-dimensional spins arranged on a 2-dimensional mesh are relaxed using a Landau-Lifshitz ordinary differential equation solver. A magnetic field is applied to the system and each spin is allowed to precess, under the action of the total field acting on that spin and a damping term, in accordance with the Landau-Lifshitz equation. The total field acting on a spin is composed of the applied field and effective fields representing magnetocrystalline anisotropy, exchange and self-magnetostatic energies. The system is allowed to evolve until the total torque on all spins is below an arbitrary limit. The presented model was modified from the code available from NIST by allowing the material parameters — saturation magnetization (M_s), magnitude and direction of the uniaxial magnetocrystalline anisotropy (K) and exchange parameter (A) — to vary from spin to spin. In this way a granular structure could be simulated and the properties of the system examined as the degree of easy axis alignment was varied.

The material simulated consisted of a two-dimensional slice of $Nd_2Fe_{14}B$, 600 nm long in the x-direction by 300 nm high in the y-direction. Two different schema were used for the simulation, each consisting of 18 grains in total. In the first scheme — the isotropic case — the easy axis of each grain was chosen randomly to lie in the plane of the slice. In the second scheme — the anisotropic case — the easy axis of each grain was chosen to lie in the plane of

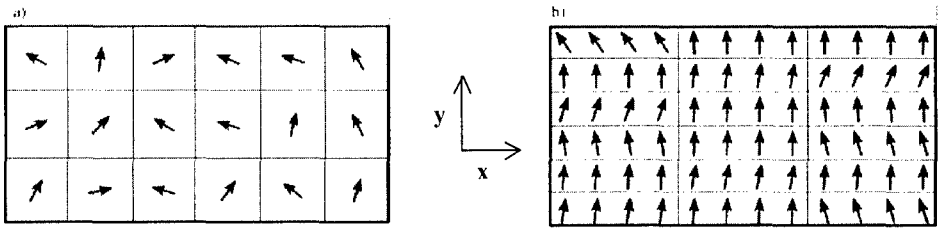

Fig. 7. Figures representing the grain boundaries and easy axis directions for the two schema described in the text. The field was applied such that the x-component was $1/6^{th}$ the y-component in magnitude, which is approximately 9.5° from the y-direction. a) The isotropic scheme. The grains dimensions are 100 nm by 100 nm and the total simulation is 600 nm by 300 nm. b) The anisotropic scheme. The grains dimensions are 200 nm by 50 nm and the total simulation is the same size as a).

the slice from a Gaussian distribution with a standard deviation of 10° about the y-direction. These easy axis distributions simulate, in two dimensions, the experimental easy axis distributions found in hot-pressed and optimally die-upset magnets respectively [6]. In the isotropic scheme each of the 18 grains was 100 nm by 100 nm in size. In the anisotropic scheme each of the 18 grains was 200 nm by 50 nm in size. The change in shape corresponds to that produced by the die-upsetting procedure which is used to develop crystallographic and magnetic texture in melt-quenched $Nd_2Fe_{14}B$. For simplicity the grain size was the same for all grains in each scheme. The directions of the easy axes and the positions of the grain boundaries are shown in Fig. 7 for the two schema considered in this work. The magnetic field was applied in the plane of the slice with a y-component 6 times that of the x-component. A full three-dimensional treatment was used in the self-magnetostatic energy calculation, known as the "3Dslab" calculation in the OOMMF code. The computational cell size chosen for the simulations was 1.5 nm, which is sufficiently small to allow accurate modeling of domain walls in $Nd_2Fe_{14}B$. The physical properties chosen for $Nd_2Fe_{14}B$ were M_s = 1274 kA/m, A = 100 pJ/m, K =5 MJ/m^3. The exchange parameter across the grain boundary was assumed to be equal to the bulk value to simulate the upper limit of exchange coupling possible.

Normalized hysteresis loops for the demagnetization section of the curve for the two schema considered are shown in Fig. 8. The isotropic curve has a remanence above the expected value of 0.5 because only 18 grains were considered in the simulation, a number that is too small to allow proper statistical sampling of the isotropic distribution. The remanence of the anisotropic curve is much larger, consistent with the aligned nature of the texture distribution assumed. The coercivity of the anisotropic curve is nearly twice that of the isotropic curve, contrary to experimental findings. However, in micromagnetic simulations the coercivity is expected to increase as the degree of alignment increases because the nucleation field increases as the applied field is aligned more nearly with the easy axis of the grain [22]. The calculated form of the demagnetization curve is more diagnostic of the effect of intergranular alignment. The isotropic curve shows a two-stage magnetic reversal, the first reversal occurring at 1 T with the second reversal occurring at a higher field of 2 T. For the anisotropic curve, apart from a small amount of reversible rotation which occurs in larger negative fields, the entire reversal occurs in a single jump at H = 4 T.

The reasons underlying the two-stage reversal process in the isotropic case were revealed once the magnetization distributions at each field were examined. The magnetization distribu-

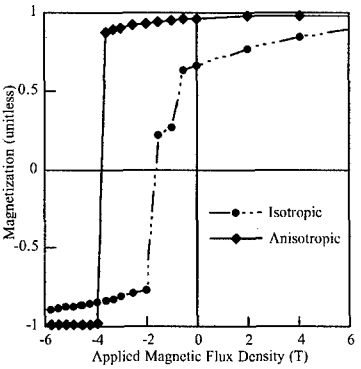

Fig. 8. Second-quadrant normalized hysteresis loops for the isotropic and anisotropic schema. The isotropic case displays a two-stage reversal while the anisotropic case displays only a single-stage reversal.

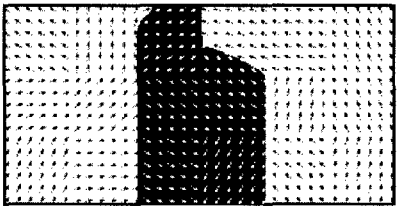

Fig 9. Magnetization distribution in a stable state at 1.5 T for the isotropic scheme. The arrows represent average magnetization of a 12 x 12 element square; black-white shading represents parallel or anti-parallel polarization to the applied field. Domain walls can be seen crossing the two upper grains of the black shaded region.

tion for the isotropic scheme in a field of 1.5 T is shown in Fig. 9. Although the first nucleation event occurred at a field of 1 T, only a portion of the grains in the isotropic material were reversed by this nucleation, in contrast to the reversal of the anisotropic material. It may be concluded that not only does grain misalignment lower the remanence of the ensemble, it also reduces the exchange length that communicates the magnetization information from grain to grain and changes the scale of the interaction domains. This result arises from the isotropic nature of the material with a perpendicular magnetization component at the grain peripheries that convey a reduced exchange length. This reduced exchange length is accompanied by a magnetization misalignment across the grain boundaries that pins domain walls at stray field inhomogeneities, creating smaller interaction domains by virtue of an increased density of domain wall pinning sites. It is thus seen that the grain alignment of a material has consequences not only on the coercivity and remanence, but upon the expected scale of the interaction domains as well.

SUMMARY AND CONCLUSIONS

The three experimental scenarios previously described all consistently support the hypothesis that granular alignment in nanocrystalline materials is accompanied by an increased degree and extent of magnetic exchange coupling. The increase in the exchange coupling is attributed to an increase in the magnetic exchange length L_{ex}^{0} as the interfacial perpendicular magnetization component is reduced. This increased magnetic exchange coupling increases the interaction domain size and suppresses the coercivity, although at the same time produces an exchange-enhanced remanence. An unavoidable conclusion is that high remanence and high coercivity seem to be mutually exclusive in nanocrystalline magnets.

It may, however, still be possible to engineer aligned nanocrystalline magnetic materials with a high remanence and a robust coercivity. The key to the optimal microstructure lies in the materials design, and associated processing, of the grain boundary the separates the constituent nanograins. It is necessary to keep the magnetic intergrain correlation length smaller than the exchange length L_{ex}^{0} to avoid the formation of extended interaction domains that degrade the co-

ercivity. This may be accomplished with a non-magnetic grain boundary phase of dimensions on the order of the pertinent exchange length. At the same time grain alignment is necessary to provide a large remanence via alignment of moments with a small angular dispersion about a defined axis, but not necessarily from exchange enhancement. In bulk materials these design parameters might be satisfied by the addition of as-yet unidentified elements to the $Nd_2Fe_{14}B$ base composition that would serve to both lower the melting point of the eutectic liquid phase necessary for successful die-upsetting as well as render that phase non-magnetic. In any case the attainment of the truly optimal nanostructure that provides both high remanence and high coercivity in advanced permanent magnets is a challenging task..

ACKNOWLEDGMENTS

Research performed at Brookhaven National Laboratory under the auspices of the U.S. Dept. of Energy, Division of Materials Sciences, Office of Basic Energy Sciences under contract No. DE-AC02-98CH10886.

REFERENCES

[1]. C. D. Fuerst and E. G. Brewer, *J. Appl. Phys.* **73** (1993) 5751.
[2]. H. A. Davies, *J. Magn. Magn. Mater.* **157/158** 11 (1996).
[3]. E. C. Stoner and E. P. Wohlfarth, *Philos. Trans. Roy. Soc. London A* 240 (1948) 599.
[4]. E. J. Kondorsky, *J. Exp. Theor. Fiz.* **10** (1940) 420.
[5]. D. Givord and M. F. Rossignol, "Coercivity" Ch. 5 in Rare-earth Iron Permanent Magnets, J. M. D. Coey, Ed., Clarendon Press, Oxford (1996).
[6]. L. H. Lewis, T. R. Thurston, V. Panchanathan, U. Wildgruber and D. O. Welch, *J. Appl. Phys.* **82** (7) (1997) 3430.
[7]. H. Kronmüller and T. Schrefl, *J. Magn. Magn. Mater.*, **129** (1994) 66.
[8]. Gieslher Herzer, *Materials Science and Engineering* **A133** (1991) 1.
[9]. R. C. O'Handley, Modern Magnetic Materials, John Wiley & Sons, New York (2000) 294.
[10]. J. M. D. Coey, "Introduction" Ch. 1 in Rare-earth Iron Permanent Magnets, J. M. D. Coey, Ed., Clarendon Press, Oxford (1996).
[11]. D. C. Crew, L. H. Lewis and V. Panchanathan, *J. Magn. Magn. Mater.* **223** (3) (2001) 261.
[12]. D.C. Crew, L.H. Lewis and V. Panchanathan, *J. Magn. Magn. Mater.* in press.
[13]. D. C. Crew and L. H. Lewis, *IEEE Trans. Magn.* in press.
[14]. W.F. Brown, *Rev. Mod. Phys.* **17** (1945) 15.
[15]. A. Aharoni, *Rev. Mod. Phys.* **34** (1962) 227.
[16]. S. Hirosawa and Y. Tsubokawa, *J. Magn. Magn. Mater.* **84** (1990) 309.
[17]. R. Grossinger, X.K. Sun, R. Eibler, K.H.J. Buschow and H.R. Kirchmayr, *J. Magn. Magn. Mater.* **58** (1986) 55.
[18]. D. C. Crew, L. H. Lewis, D. O. Welch, V. Panchanathan, *J. Appl. Phys.* **87** (2000) 6571.
[19]. T. Schrefl, J. Fidler and H. Kronmüller, *Phys. Rev.* **B 49** (9) (1994) 6100.
[20]. M. K. Griffiths, J. E. L. Bishop, J. W. Tucker and H. A. Davies, *J. Magn. Magn. Mater.* **183** (1998) 49.
[21]. M. J. Donohue and D. G. Porter <URL: http://math.nist.gov/oommf/> version 1.1.
[22]. T. Schrefl, H. F. Schmidts, J. Fidler, H. Kronmüller, *J. Appl. Phys.* **73** (1993) 6510-6512.